Int J Adv Manuf Technol (2013) 69:1765–1773
DOI 10.1007/s00170-013-5141-4

ORIGINAL ARTICLE

Underwater-laser drilling of aluminum

Nikša Krstulović · Sharon Shannon · Robert Stefanuik · Carlo Fanara

Received: 5 March 2013 / Accepted: 17 June 2013 / Published online: 5 July 2013

Abstract Pulsed-laser ablation of an aluminum bulk sample was performed both in water and air with a Q-switched Nd:YAG 1,064-nm laser over a range of high-output energies from 100 to 500 mJ. The effect of laser drilling in terms of produced crater volumes as a function of water-layer thickness was studied. The water-layer thickness was varied from 1 to 20 mm. In a special case, water droplets were added to the ablation region of the dry target in order to support ablation. Water-layer thickness in that case was estimated to be 0.5 mm. A comparison of the results obtained in air and underwater was performed. It is found that the aluminum target may be drilled more efficiently under the confinement of water compared to drilling in air environment. Further drilling efficiency can be achieved by varying the thickness of water. The optimized water thickness under the conditions of our experiment was found to be 3 mm. In that case, a 28-fold increase in crater volume and 18-fold increase in crater depth was achieved as compared to ablation in air. In underwater ablation, the formation of irregular surface structures of re-deposited material around the crater (rim) is avoided and the crater surface is smoother. In an air environment, the drilling is suppressed due to an immediate re-solidification and re-deposition of ablated material. This leads to a better characteristics of craters obtained underwater in terms of roughness, shape, volumes, and reproducibility.

Keywords Underwater-laser drilling · Underwater ablation · Wet ablation · Aluminum · Laser micromachining

N. Krstulović (✉) · S. Shannon · R. Stefanuik · C. Fanara
School of Physics, Science Centre North,
University College Dublin, Belfield 4, Dublin, Ireland
e-mail: niksak@ifs.hr

C. Fanara
EPPRA (European Pulsed Power Research Applications),
Avenue du Quebec 16, 91140 Villebon-sur-Yvette, France

1 Introduction

Pulsed-laser processing of materials is important for both scientific and industrial applications: laser radiation is widely applied in the micro- and nano-structuring of materials where high precision structures are desired [1–4]. Such structures require high-spatial resolution and accuracy as well as high-aspect ratio (depth to radius ratio) profiles. To obtain better performances of the material structuring, experiments were often supported by a theoretical studies [5, 6]. The laser–material coupling greatly depends on the type of medium where ablation takes place (air, vacuum, gases, liquids, gels) and affects the quality and the properties of the pulsed-laser micro-machined structures. It is well known that heat accumulation around the laser pulse-affected zone is a significant problem in the laser micro-fabrication of materials [7–9]. Heat accumulation causes several problems to micromachining:

(1) Re-deposited material around the crater (often results in a formation of very irregular crown-like structures along the crater edge, either by direct re-deposition and/or by the flow of melted material. Such structures may screen the crater from the laser pulse, making ablation difficult. The net effect is that the processing is dimensionally inaccurate).
(2) Limited depth of the drilled crater (ablated material is re-deposited back to the internal crater surface).
(3) Non-cylindrical shape of the crater profile (the crater profile often does not follow a laser Gaussian or structured intensity profile due to a poor laser–material coupling or material re-deposition).
(4) Formation of surface structures such as defects, ripples, or cracks (due to the rapid re-solidification and/or the stress induced by the laser pulse impact).

By adding a water layer onto the target surface, the formation of the melted flow and the re-deposition of ablated material may be avoided [10]. Due to its high heat capacity

and thermal conductivity (with respect to air), water prevents heat accumulation by absorbing the extra heat (0.6 W/(mK) in water against 0.025 W/(mK) in air at ambient temperature). It results in an efficient cooling of the target. Moreover, unlike in air, most of the ablated material does not re-deposit back onto the target but is carried away by the fluid motion and finally dissolves into the water.

The rapid temperature increase due to the laser pulse induces the formation of vapor bubbles and of two shock waves (one expands into the water and the other into the target) [11]. Vapor bubbles play an important role in underwater-laser drilling. They carry ablated material away from the irradiated area promoting the drilling (no scattering) and the formation of regular structures (no re-deposition) [12]. After the expansion of the shock wave a cavitation bubble is generated due to the expansion of the ablated material. Upon the collapse of the cavitation bubble when its diameter reaches a maximum (few millimeters), a high-speed and high-pressure liquid jet is formed and directed towards the target surface followed by a secondary shock wave [13]. The liquid jet provides a mechanical impact (high-pressure impact) onto the target surface, improving the drilling rate [14]. At the boundary between the water and air, the shock wave induced in the water is reflected back to the target surface providing an additional impact thereby enhancing the drilling rate. Underwater laser-produced plasmas have a reduced lifetime and are confined to a small volume. This reduces the plasma-laser shielding, which increases the ablation rate due to the improved acoustic coupling [15]. To summarize, the net effect of adding water above the target surface during laser ablation is a greatly improved drilling rate and precision for dimensional structuring [16]. The process of laser ablation when the target is immersed into water or affected by water droplets is called "wet ablation" (underwater or water-assisted). It is in contrast to "dry ablation" where the target is exposed to a vacuum or an air environment.

The above mentioned advantages and the relatively simple experimental set-up allow wet ablation to contribute to a wide variety of applications including drilling, micro-milling, cutting, 2D and 3D structuring, engraving, welding, etching, and plasma spraying for nanostructured coatings, which are not limited to metallic materials [17–21]. Underwater-laser ablation is found to be a versatile technique for the production of nanostructures and can serve as a source of nanoparticles [22], nanoclusters [23], and nanocrystals [24, 25] of various chemical elements and for various purposes [26–30]. The efficiency of wet ablation depends on the experimental parameters such as laser-pulse wavelength, fluence, duration, number of laser pulses [31–34], liquid species [35], and liquid-layer thickness [36]. In most of the literature cited above, the enhancement of wet ablation as compared to the case of dry ablation in air is reported. Nevertheless, longer laser pulses (millisecond pulses) may result in the decrease of wet ablation efficiency [37, 38].

In the present work, nanosecond laser pulses were used and the efficiency of wet laser ablation was studied on aluminum. The influence of water-layer thickness (0.5–20 mm) on the drilling rate and the crater structure of aluminum was investigated with respect to drilling in air. In a special case, drops of water were added onto the irradiated area using a pipette. The effect of varying the water-layer thickness was investigated and an optimal determined for the highest drilling rate.

2 Experimental setup

Experiments were carried out using a Q-switched Nd:YAG laser operating at 1,064 nm with a repetition rate of 5 Hz and with a pulse duration of 18 ns at full-width at half-maximum (FWHM) (Spectron SL805). In order to study the drilling rate, the output energy was varied from 100 to 500 mJ, while the number of applied pulses was varied from 10 to 1,000. The laser beam was focused onto the target surface with a 10-cm lens. The experimental setup is shown in Fig. 1. Fig. 1a represents drilling schematics underwater, where h denotes the water thickness above the target surface. Fig. 1b represents water droplet-assisted ablation in which water droplets were added into the ablation region using a pipette in order to ensure a wet ablation area during the drilling process (estimated thickness of the water layer in this case is 0.5 mm). The frequency of droplets released from the pipette was at an approximately 3 Hz. The drilling sample was a 3-mm thick sheet of aluminum of dimensions 2×2 cm, immersed in purified water (Milli-Q). The sample was placed in a 500-ml glass container. In order to optimize the drilling efficiency, h was varied from 1 to 20 mm.

The crater semi-profiles were obtained using a fluorescent microscope. The images were recorded at consecutive focal microscope positions (at certain depth points in the crater) starting from the top of the crater (equal to the target surface) towards the bottom. From each picture, the radius of the crater was determined. The difference of the focal positions between the top and bottom images defines the total depth of a crater, d. The plot of the focal positions vs. the obtained radii gives the crater semi-profiles used to calculate their volumes. A scanning electron microscope (SEM) was used to make an overall image of the craters due to its relatively broad focus. The SEM images allowed the inspection of the morphology of a given surface.

3 Results and discussion

Figure 2 shows the SEM images of the craters obtained with 1000 laser pulses in air (a and b) and underwater (c and d). The layer thickness of water was h=10 mm and the output

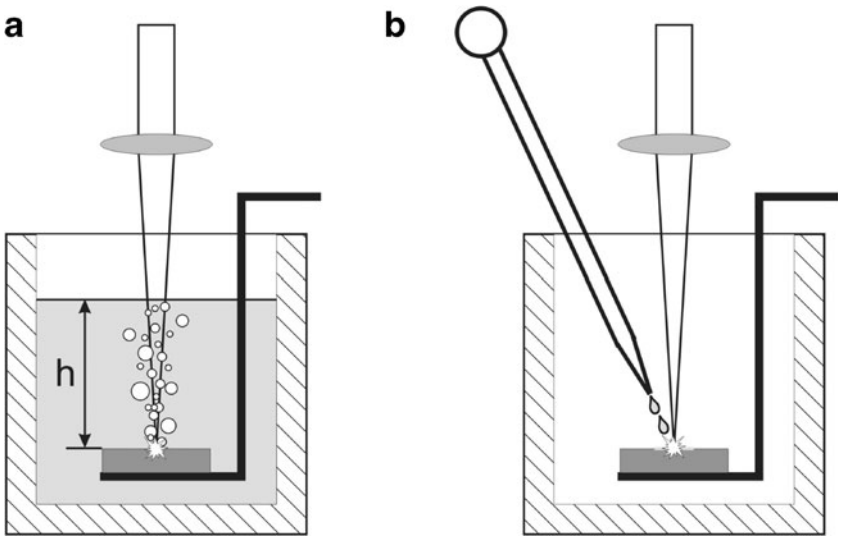

Fig. 1 Experimental scheme **a** underwater drilling and **b** water droplet-assisted drilling

laser-pulse energy 500 mJ. It can be seen that drilling in air leads to the formation of irregular shallow craters with an undefined shape. The area of these irregular structures is much larger than the area affected by the focused laser pulse (250–300 μm). It suggests that the rapid re-deposition of ablated material occurred as a result of the action of the high-pressure ablation plume on the melted target surface. Furthermore, thermal diffusion of the heat induced in the material by the laser pulse also contributes to the formation of such irregular structures. The heat-affected zone becomes larger than the irradiated area. It results in the melting of the target material outside the irradiated area. Re-solidification and accumulation of such materials makes the crater edge irregular. All these effects make dry cratering or drilling (material removal) inefficient and impractical. In contrast, Fig. 2c and d show how wet ablation provides craters of regular and reproducible shapes with a significant increase in the drilling rate in comparison to dry ablation. At the micrometer-sized scale the crater surfaces differ significantly in wet and dry ablation. While the surface structure is irregular and locally smooth in the case of dry ablation (Fig. 2b), in wet ablation, the crater surface is flat and contains micron-sized periodic ripples (Fig. 2d) caused by bubbles collapse near the target surface as mentioned before [13].

Figure 3 shows the SEM images of craters obtained after 10, 50, 100, and 300 pulses with output energy of 500 mJ. The images were taken at an angle of 45 ° with respect to the target surface normal. The images depict the formation of a

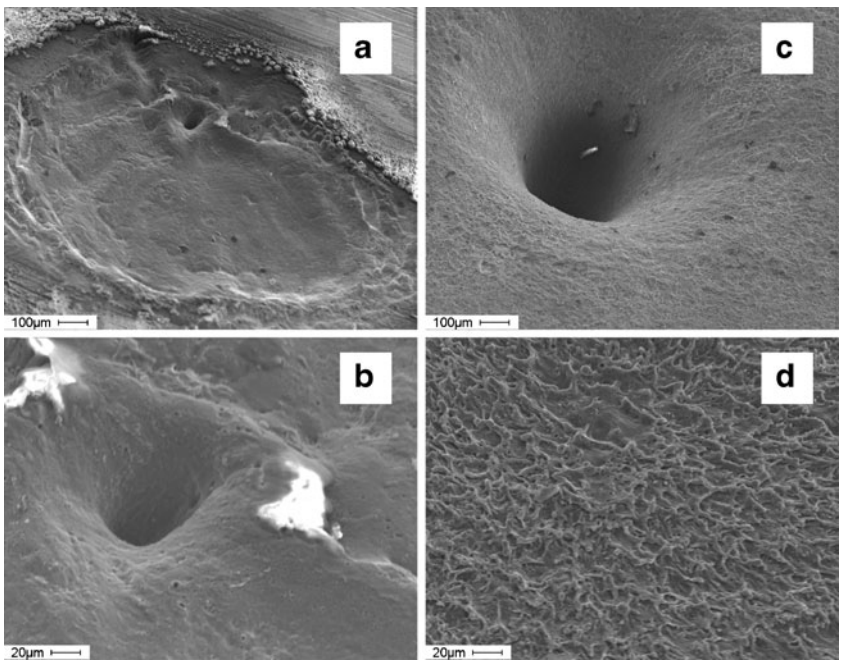

Fig. 2 SEM images of Al craters obtained with 1,000 pulses **a**, **b** in air and **c**, **d** underwater (h=10 mm). Images were taken at a 45 ° angle with respect to the surface normal

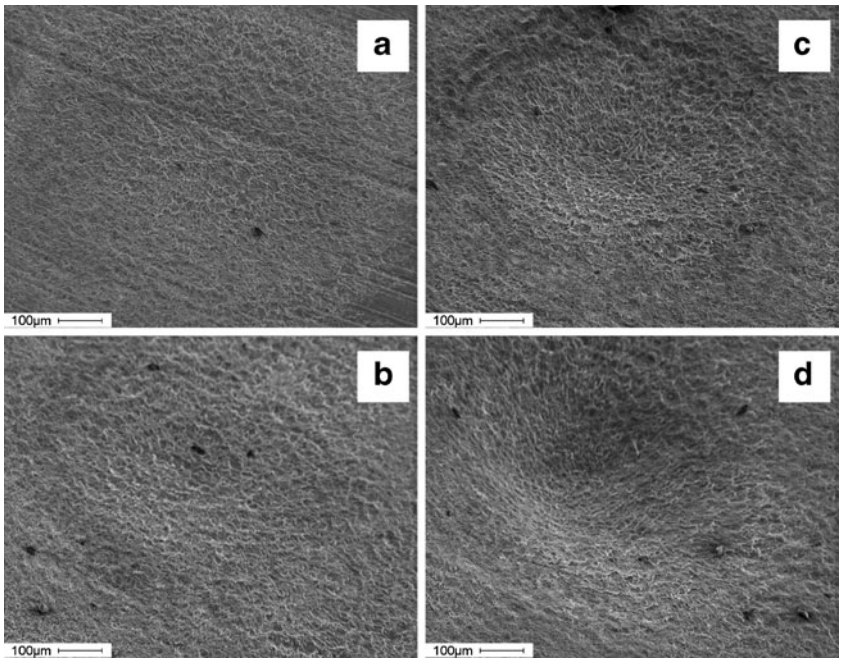

Fig. 3 The SEM images of Al craters obtained under water (h=10 mm) with **a** 10, **b** 50, **c** 100, and **d** 300 pulses. Images were taken at a 45 ° angle with respect to the surface normal

crater in the initial stage of the drilling process. It is evident that there is no recast material during the process of drilling. The surface of the crater became rippled even after a few laser shots. The ripples were formed with slight preferential direction from the center of the crater towards the edge. This is evidence of the pressure-induced effect on the laser-heated target underwater (cavitation bubble collapse). The pressure is highest at the center of the crater and decreases radially.

Figure 4 shows an SEM image of a crater in the final stage of drilling after 1,000 pulses. The image was taken at normal incidence with respect to the target surface (top-to-bottom). The crater shape is regular and sharp while the internal surface is rippled and smooth, indicating there is no re-deposited material in any stage of the drilling process. Note that impurities are present on the crater due to ablated micro-material precipitation during the processing or dust collection during the SEM preparation.

To quantify the ablation efficiencies and to inspect the crater shapes, crater profiles (crater depth vs. radius) were studied. Figure 5 shows crater semi-profile cross-sections for water thicknesses between 1 and 20 mm for (a) 1,000 and (b) 300 applied laser pulses with 500 mJ of output energy. Figure 5 also exhibit crater semi-profiles obtained in air and distinctly by adding water droplets using a pipette. In all cases, wet ablation resulted in a significant enhancement of crater volumes, depths, and shapes. As shown in Fig. 5, the crater depth and consequently the volume, depend on the water-layer thickness. In contrast to dry ablation, all craters obtained in water have Gaussian-like profiles, which follow the specified laser pulse shape.

In Fig. 6, the dependence of the crater volume and depth on the water-layer thickness is shown. The calculation of the volumes and the depths is based on the crater semi-profiles shown in Fig. 5. It was found that both the crater volume and depth vary with the thickness of the water layer (a similar dependence on the water-layer thickness was found in [39] for the case of the ablation of silicon with KrF laser). Figure 6 shows that the maximum volume and depth was reached for water thickness of 3 mm. In this case, the volume enhancement factor (wet to dry ablated volume ratio) is 28 and 13 for 1,000 and 300 applied pulses, respectively. The equivalent depth enhancement factors are 18 and 14 for 1,000 and 300 applied pulses, respectively. The volume and depth enhancements are not a linear function of the number of applied pulses; this is related to the difficulties of producing dry craters which are used for normalization of the enhancement. For water thicknesses lower than 3 mm, the enhancement is limited but still evident. This is related to weaker plasma

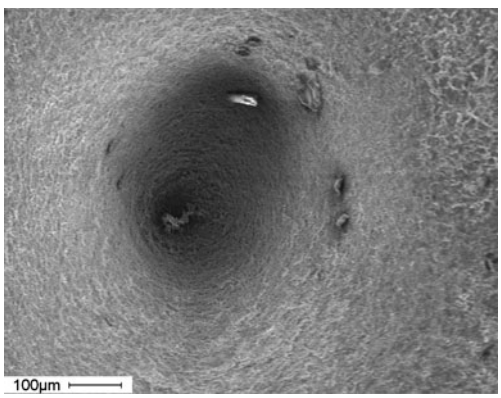

Fig. 4 An SEM image of an Al crater obtained underwater (h=10 mm) with 1,000 pulses. Images were taken at normal incidence with respect to the target surface

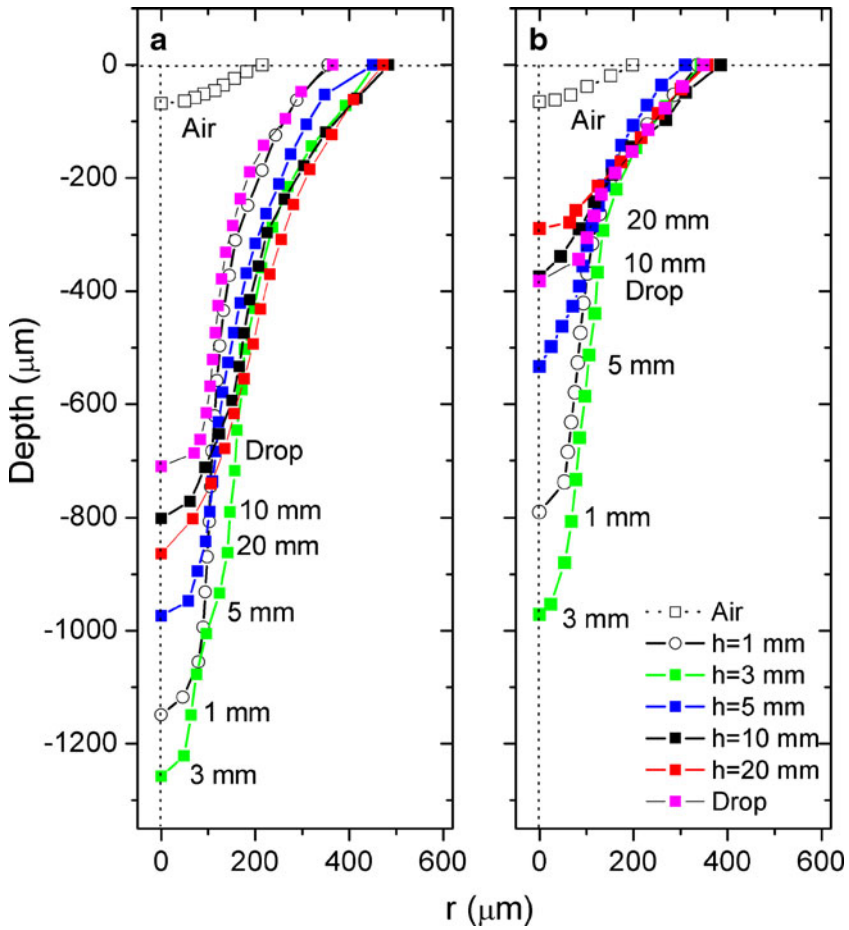

Fig. 5 The crater semi-profiles obtained with different water thicknesses with **a** 1,000 and **b** 300 pulses. Repetition rate 5 Hz, pulse energy 500 mJ (*x* and *y* axis are to scale). The crater produced in air is shown for comparison

confinement by the water layer [16] and by the shock waves and cavitation bubble dynamics [13]. For low thicknesses, the shock waves may not be fully developed thus never reaching the maximum pressure. The expansion of cavitation bubble may be disturbed by the low thickness of the water layer and it will not collapse after reaching the maximum in diameter and in pressure. As a consequence, the high-speed liquid jet formed after the cavitation bubble collapse is weaker and the pressure back-impact to the target decreased. The other effect apparent at low h is that the laser-pulse impact causes a removal of a certain amount of water above the target [19]. This changes the plasma confinement and consequently the drilling rate. For the drop layer of 0.5 mm, the enhancement is about 10 times which implies that even a thin-liquid film can significantly improve the ablation rate [40]. In contrast, for water-layer thicknesses higher than 3 mm, the plasma is estimated to be better confined while the water layer remains flat during laser drilling (not disturbed by the laser-pulse impact) but other processes may take place. Namely, the laser pulses travel a longer pathway to reach the target and hence are more scattered by the debris or the micro- and nano-particles and by the induced bubbles emerging from the target surface. Due to the longer pathway, the shock wave reflected from the air-water boundary back to the target surface is weakened, which decreases the drilling rate. Those two effects are evident from Fig. 6, as a slight decrease in the volumes and the depths, as the water layer thickness is increased. The total overview of achieved drilling enhancements with regard to the crater volumes and depths can be seen in Fig. 7. All values shown in Fig. 6 are normalized to the values obtained in air for the quantification of the enhancements.

The crater semi-profiles obtained with various numbers of pulses (100, 300, 500, and 1,000 pulses) and different pulse energies (100, 300, and 500 mJ) are shown in Fig. 8. Measurements were made with a layer thickness of 10 mm. For the given set of parameters, the crater depths increase with both the laser energy and the number of delivered pulses. The crater radius on the top of the target surface increases from 250 to 400 μm by increasing the number of pulses for the 500 mJ case. For 300 and 100 mJ, the crater radius is roughly constant, around 250 and 175 μm for 300 and 100 mJ, respectively. The laser-pulse fluences can be estimated using the values of the surface crater radii and the pulse energy. We find fluences of 80, 150, and 200 J/cm^2 for the pulse energies of 100, 300, and 500 mJ, respectively.

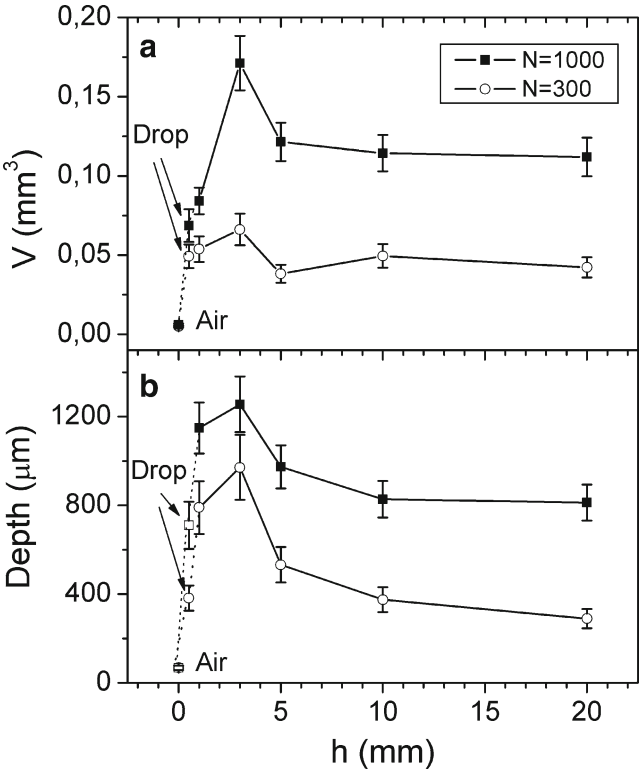

Fig. 6 **a** The crater volumes and **b** the crater depth vs. water thickness for a different number of pulses. The volume of the crater produced in air is shown for comparison

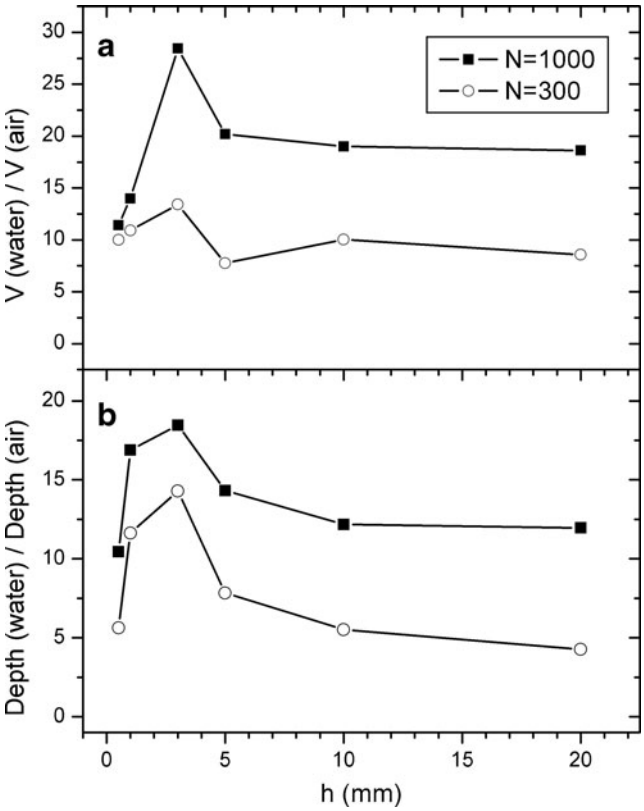

Fig. 7 **a** The volume and **b** the depth enhancement ratios of the craters obtained at different water-layer thicknesses with respect to the volumes and the depths obtained in air, respectively

All values of the crater volumes and depths are summarized in Fig. 9. It can be seen that the volume is a linear function of the number of pulses with laser-pulse energy of 500 mJ. In the other two cases, the increasing trend is less pronounced. All depths investigated depend on the number of pulses in a similar way and are linear below 500 pulses. The drilling enhancement is related to the laser-induced plasma confinement, especially at the higher laser energies. In fact, it was observed that due to the lateral thermal diffusion, the higher the plasma intensity, the larger the affected area is. This statement is based on the significantly larger crater radius obtained with 500 mJ as drilling continues. In addition, the internal crater radius also increases with the number of pulses, which is not the case for 300 and 100 mJ, where the internal radii do not vary significantly during drilling. Thus, the crater volume at higher pulse energy increases as both the internal crater radii and depth increase, which make drilling significantly more efficient. At lower energies, the crater volumes increase mostly due to an increase in the crater depth, while the internal crater radii remain constant. This explains the higher steepness of the crater volume vs. number of pulses curve for the 500 mJ case in Fig. 9a with respect to the curves related to the 300 and 100 mJ cases.

To quantify the crater aspect ratio, a Gaussian fit of the crater profiles was performed. A FWHM was obtained from the fit and used as a typical crater radius (r_{FWHM}) for the calculation. The fit is performed on the crater profiles shown in Figs. 5 and 8. The results are shown in Fig. 10. In Fig. 10a, it is shown how d/r_{FWHM} depends on the water-layer thickness for 1,000 and 300 pulses for the pulse energy of 500 mJ. The case $h=0$ mm represents the crater obtained in air. It is evident that the highest d/r_{FWHM} is achieved for the $h=1$ mm and 1,000 pulses and its value is 10. For 300 pulses, the maximum of d/r_{FWHM} is achieved for $h=3$ mm and its value is 9. The d/r_{FWHM} dependence on h shows similar behavior to the drilling rate enhancement dependence on h. This implies that the crater profiles have the best aspect ratio (highest d/r_{FWHM}) when they are drilled with a highest drilling rate (highest d). The d/r_{FWHM} dependence on the number of pulses for three pulse energies is shown in Fig. 10b where $h=10$ mm. This dependence shows a similar linear trend for all energies. The aspect ratio of the drilled crater does not depend on the applied pulse energy significantly.

4 Conclusions

Underwater drilling of aluminum was studied with respect to dry drilling in air. In comparison to dry ablation, the drilling rate obtained with wet ablation is enhanced in terms of the crater

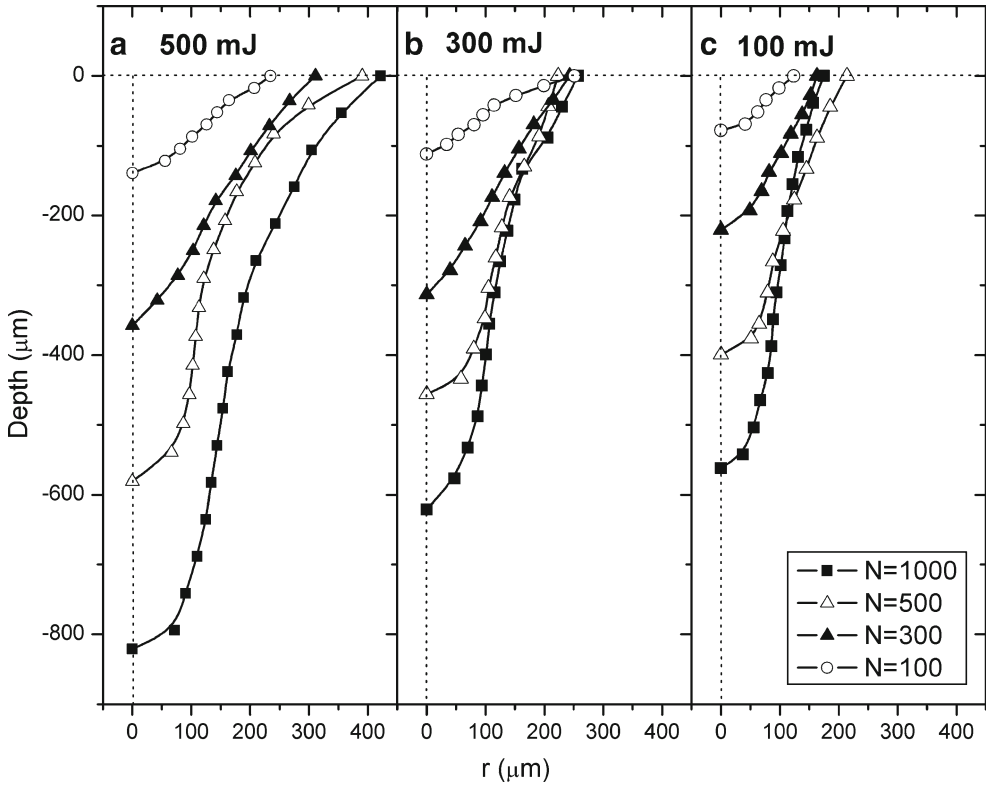

Fig. 8 The crater profiles obtained at different pulse energies **a** 500 mJ, **b** 300 mJ, and **c** 100 mJ for different numbers of pulses. Water thickness h=10 mm

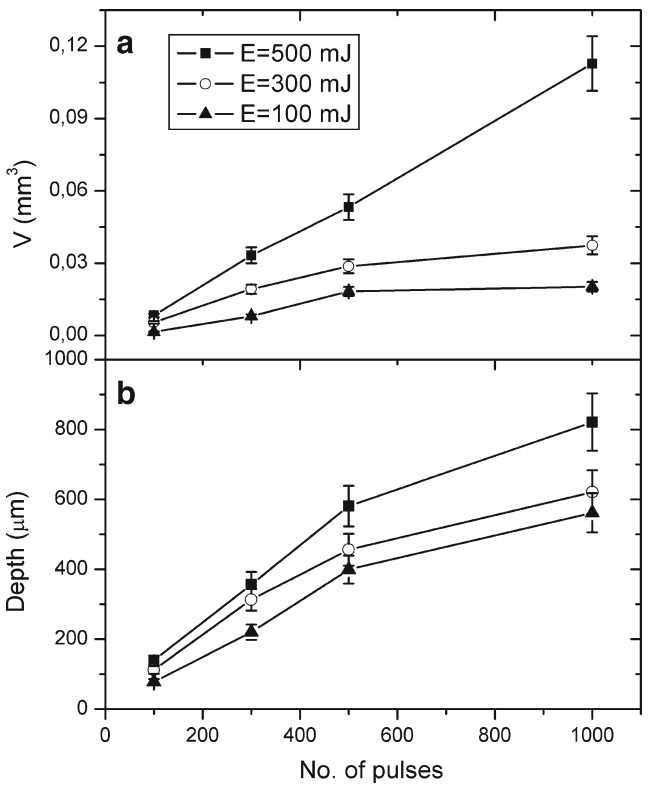

Fig. 9 **a** The volumes and **b** the crater depth vs. various number of pulses for three different energies. Water thickness h=10 mm

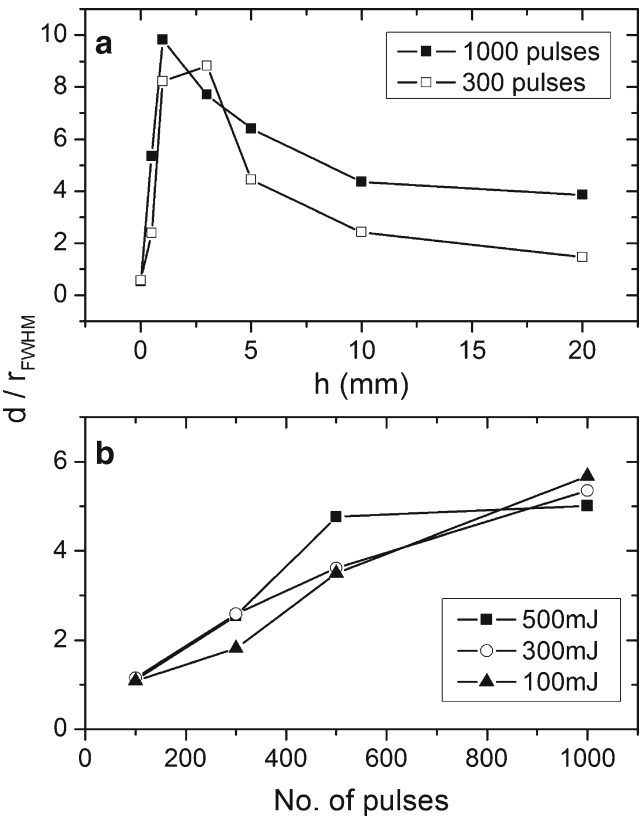

Fig. 10 Aspect ratios obtained at different **a** water thicknesses for 300 and 1,000 pulses and **b** number of pulses for three different energies. Water thickness h=10 mm

depth and volume, while the crater shape quality is significantly improved. The drilling enhancement is related to better laser-target coupling and to additional effects such as the limitation of heat accumulation, the removal of debris that avoid re-deposition, and the mechanical impact related to the formation and the collapse of bubbles of evaporated material.

The underwater drilling rate is further improved by varying the water-layer thickness. It is found that in this experiment, the drilling is most enhanced for a 3-mm thick water layer.

The crater shape obtained underwater for any water-layer thicknesses is regular and follows the laser-pulse Gaussian intensity profile. The crater surface is rippled and rough having a dendritic structure and of better quality and regularity than the surface obtained in dry ablation. The d/r_{FWHM} depends much more on the water thickness than on the applied pulse energy.

Underwater-laser ablation/drilling is a promising and cost-effective technique for fast drilling and surface modification not only for metals, but for many other materials. In comparison to ablation in air, the underwater-laser ablation allows drilling of craters (holes) with better resolution and quality as well as with higher processing speed (higher efficiency).

Acknowledgments This work is funded by SFI under grant number 08/RFP/PHY1180 and by EU-MC-IAPP FIRE Project No: 230726; and under the SFI-Equipment Award and UCD Strategic and Major Initiative Scheme. We also like to acknowledge the kind support of the mechanical workshop at the School of Physics, UCD.

References

1. Li L, Hong M, Schmidt M, Zhong M, Mashe A, Huis int'Veld B, Kovalenko V (2011) Laser nano-manufacturing–state of the art and challenges. CIRP Annals - Manufacturing Technology 60(2):735–755
2. Dubey AK, Yadava V (2008) Laser beam machining—a review. Int J Mach Tool Manuf 48:609–628
3. Knowles MRH, Rutterford G, Karnakis D, Ferguson A (2007) Micro-machining of metals, ceramics and polymers using nanosecond lasers. Int J Adv Manuf Technol 33:95–102
4. Chryssolouris G, Tsoukantas G, Salonitis K, Stavropoulos P, Karagiannis S (2003) Laser machining modelling and experimentation—an overview, Proc SPIE 5131, 3rd GR-I International Conference on New Laser Technologies and Applications 158–168
5. Stournaras A, Salonitis K, Stavropoulos P, Chryssolouris G (2009) Theoretical and experimental investigation of pulsed laser grooving process. Int J Adv Manuf Technol 44:114–124
6. Salonitis K, Stournaras A, Tsoukantas G, Stavropoulos P, Chryssolouris G (2007) A theoretical and experimental investigation on limitations of pulsed laser drilling. J Mater Process Technol 183:96–103
7. Hopp B, Smausz T, Bereznai M (2007) Laser drilling of high aspect ratio holes in copper with femtosecond, picosecond and nanosecond pulses. Appl Phys A 61:77–79
8. Weck A, Crawford THR, Wilkinson DS, Haugen HK, Preston JS (2008) Laser drilling of high aspect ratio holes in copper with femtosecond, picosecond and nanosecond pulses. Appl Phys A 90:537–543
9. Krstulović N, Milošević S (2010) Drilling enhancement by nanosecond–nanosecond collinear dual-pulse laser ablation of titanium in vacuum. Appl Surf Sci 256:4142–4148
10. Kang HW, Lee H, Welch AJ (2008) Laser ablation in liquid-confinement using a nanosecond laser pulse. J Appl Phys 103:083101
11. Vogel A, Busch S, Parlitz U (1996) Shock wave emission and cavitation bubble generation by picoseconds and nanosecond optical breakdown in water. J Acoust Soc Am 100:148–165
12. Ohara J, Nagakubo M, Kawahara N, Hattori T (1997) High aspect ratio etching by infrared laser induced micro bubbles. The Tenth Annual International Workshop on Micro Electro Mechanical Systems. 26-30 Jan 1997.
13. Tsuji T, Okazaki Y, Tsuboi Y, Tsuji M (2007) Nanosecond time-resolved observations of laser ablation of silver in water. Jpn J Appl Phys 46:1533–1535
14. Isselin JC, Alloncle AP, Autric M (1998) On laser induced single bubble near solid boundary: contribution to the understanding of erosion phenomena. J Appl Phys 84:5766–5771
15. Kang HW, Lee H, Chen S, Welch AJ (2006) Enhancement of bovine bone ablation assisted by a transparent liquid layer on a target surface. IEEE J Quantum Electron 42:633–642
16. Lu J, Xu RQ, Chen X, Shen ZH, Ni XW, Zhang SY, Gao CM (2004) Mechanisms of laser drilling of metal plates underwater. J Appl Phys 95:3890–3894
17. Kruusing A (2004) Underwater and water-assisted laser processing: part 2—etching, cutting and rarely used methods. Opt Lasers Eng 41:329–352
18. Choo KL, Ogawa Y, Kanbargi G, Otra V, Raff LM, Komanduri R (2004) Micromachining of silicon by short-pulse laser ablation in air and under water. Mat Sci Eng A–Struct 372:145–162
19. Tsai C-H, Li C-C (2009) Investigation of underwater laser drilling for brittle substrates. J Mater Process Technol 209:2838–2846
20. Yan Y, Li L, Sezer K, Wang W, Whitehead D, Ji L, Bao Y, Jiang Y (2011) CO2 laser underwater machining of deep cavities in alumina. J Eur Ceram Soc 31:2793–2807
21. Wee LM, Ng EYK, Prathama AH, Zheng H (2011) Micro-machining of silicon wafer in air and under water. Opt Laser Technol 43:62–71
22. Kumar B, Treja RK (2010) Synthesis of nanoparticles in laser ablation of aluminium in liquid. J Appl Phys 108:1–6
23. Perez D, Béland LK, Deryng D, Lewis LJ, Meunier M (2008) Numerical study of the thermal ablation of wet solids by ultrashort laser pulses. Phys Rev B 77:014108
24. Perminov PA, Dzhun IO, Ezhov AA, Zabotnov SV, Golovan LA, Ivlev GD, Gatskevich EI, Malevich VL, Kashkarov PK (2011) Creation of silicon nanocrystals using the laser ablation in liquid. Laser Phys 21:801–804
25. Yang GW (2007) Laser ablation in liquids: applications in the synthesis of nanocrystals. Prog Mater Sci 52:648–698
26. Kazakevich PV, Simakin AV, Voronov VV, Shafeev GA (2006) Laser induced synthesis of nanoparticles in liquids. Appl Surf Sci 252:4373–4380
27. Zhu XP, Suzuki T, Nakayama T, Suematsu H, Jiang W, Niihara K (2006) Underwater laser ablation approach to fabricating monodisperse metallic nanoparticles. Chem Phys Lett 427:127–131
28. Liu P, Cui H, Wang CX, Yang GW (2010) From nanocrystal synthesis to functional nanostructure fabrication: laser ablation in liquid. Phys Chem Chem Phys 12:3942–3952
29. Nikolov AS, Nedyalkov NN, Nikov RG, Atanasov PA, Alexandrov MT (2011) Characterization of Ag and Au nanoparticles created by nanosecond pulsed laser ablation in double distilled water. Appl Surf Sci 257:5278–5282
30. De Giacomo A, De Bonis A, Dell'Aglio M, De Pascale O, Gaudiuso R, Orlando S, Santagata A, Senesi GS, Taccogna F, Teghil R (2011) Laser ablation of graphite in water in a range of pressure from 1 to 146 atm using single and double pulse techniques for the production of carbon nanostructures. J Phys Chem C 115:5123–5130

31. Dupont A, Caminat P, Bournot P (1995) Enhancement of material ablation using 248, 308, 532, 1,064 nm laser pulse with a water film on the treated surface. J Appl Phys 78:2022–2028
32. Tunna L, O'Neill W, Khan A, Sutcliffe C (2005) Analysis of laser micro drilled holes through aluminium for micro-manufacturing applications. Opt Lasers Eng 43:937–950
33. Zhu S, Lu YF, Hong MH, Chen XY (2001) Laser ablation of solid substrates in water and ambient air. J Appl Phys 89:2400–2403
34. Berthe L, Fabbro R, Peyre P, Bartnicki E (1999) Wavelength dependent of laser shock-wave generation in the water-confinement regime. J Appl Phys 85:7552–7555
35. Kovalchuk T, Toker G, Bulatov V, Schechter I (2010) Laser breakdown in alcohols and water induced by λ=1,064 nm nanosecond pulses. Chem Phys Lett 500:242–250
36. Kang HW, Welch AJ (2007) Effect of liquid thickness on laser ablation efficiency. J Appl Phys 101:083101
37. Ageev VA, Bokhonov AF, Zhukovskii VV, Yankovskii AA (1997) Dynamics of processes occurring in laser ablation of metals in a liquid. J Appl Spectrosc 64:683–688
38. Sakka T, Masai S, Fukami K, Ogata YH (2009) Spectral profile of atomic emission lines and effects of pulse duration on laser ablation in liquid. Spectrochim Acta B 64:981–985
39. Zhu S, Lu YF, Hong MH (2001) Laser ablation of solid substrates in a water-confined environment. Appl Phys Lett 79:1396–1398
40. Kim D, Oh B, Lee H (2004) Effect of liquid film on near-threshold laser ablation of a solid surface. Appl Surf Sci 222:138–147